SIMULATION OF TURBULENT TRANSONIC SEPARATED FLOW OVER AN AIRFOIL

By George S. Deiwert, John B. McDevitt, and Lionel L. Levy, Jr.

NASA Ames Research Center

SUMMARY

A code has been developed for simulating high Reynolds number transonic flow fields of arbitrary configuration. This code, in conjunction with laboratory experiments, is being used to devise and test turbulence transport models which may be suitable in the prediction of such flow fields, with particular emphasis on regions of flow separation. The solutions describe the flow field, including both the shock-induced and trailing-edge separation regions, in sufficient detail to provide the profile and friction drag.

INTRODUCTION

Transonic flow fields over airfoil configurations are characterized by regions of subsonic flow and regions of supersonic flow. These regions are often separated by standing shock waves. If these shocks are strong enough, flow separation will occur where the shock impinges on the airfoil surface. In addition, separation is likely to occur near the airfoil trailing edge. If the Reynolds number is large, the flow will be turbulent near the airfoil surface and, in all cases, will be turbulent in the far wake.

To simulate such flow fields numerically, it is necessary to use a set of equations capable of supporting a description of all the above phenomena. In the present study the two-dimensional time-averaged Navier-Stokes equations for compressible flow are used. The Reynolds stresses are described by an algebraic eddy-viscosity model and the resulting system is solved by the second-order-accurate explicit difference method developed by MacCormack (refs. 1 and 2).

This paper describes the progress made to date in the development of such a code, the procedure used to validate the code, and the adaptation of the code to advanced computers. Solutions are shown and compared with experiments for the flow field over an 18-percent-thick, biconvex, circular-arc airfoil at zero angle of attack for several values of free-stream Mach number and chord Reynolds number.

SYMBOLS

c	chord length
C_f	skin-friction coefficient
C_p	pressure coefficient
e	internal energy per unit volume
k	thermal conductivity coefficient
ℓ	mixing length
M_∞	free-stream Mach number
p	pressure
Pr	Prandtl number
Pr_t	turbulent Prandtl number
Re_c	chord Reynolds number
s	scalar area
S	integrated surface area
t	time
T	temperature
u,v	velocity vector components in x- and y-direction, respectively
vol	integrated volume element
μ	coefficient of molecular viscosity
ρ	mass density
σ	normal stress
τ	shear stress

Subscript:

w	wall surface

Superscript:

$+$	denotes nondimensionalized boundary-layer quantity

SIMULATION METHOD

Governing Equations

The flow field is described by the two-dimensional compressible equations of motion for turbulent flow. Written in time-dependent integral form, they are:

$$\frac{\partial}{\partial t}\int_{vol} U \, d\,vol + \int_{S} \vec{H}\cdot\vec{n}\, ds = 0 \tag{1}$$

where

$$U \equiv \begin{bmatrix} \rho \\ \rho u \\ \rho v \\ e \end{bmatrix} \qquad \vec{H} \equiv \begin{bmatrix} \rho\vec{q} \\ \rho u\vec{q} + \vec{\vec{\tau}}\cdot\vec{e}_x \\ \rho v\vec{q} + \vec{\vec{\tau}}\cdot\vec{e}_y \\ e\vec{q} + \vec{\vec{\tau}}\cdot\vec{q} - k\Delta T \end{bmatrix}$$

$$\vec{q} \equiv u\vec{e}_x + v\vec{e}_y$$

$$\vec{\vec{\tau}} \equiv \sigma_x \vec{e}_x\vec{e}_x + \tau_{xy}\vec{e}_x\vec{e}_y + \tau_{yx}\vec{e}_y\vec{e}_x + \sigma_y\vec{e}_y\vec{e}_y$$

and $\vec{e}_x$, $\vec{e}_y$ are unit vectors, and $\vec{n}$ is a unit normal vector. These equations can be solved in the orthogonal x,y coordinate system for an arbitrary quadrilateral volume element (sketch (a)) by application of the split Ly and Lx operators in the manner described by MacCormack (ref. 2).

Ly operator:

$$\text{predictor} \quad \overline{U^{n+1/2}_{i,j}} = U^{n}_{i,j} - \frac{\Delta t}{vol_{i,j}}\left(\vec{H}^{n}_{i,j}\cdot\vec{S}_3 + \vec{H}^{n}_{i,j-1}\cdot\vec{S}_1\right)$$

$$\text{corrector} \quad U^{n+1/2}_{i,j} = \frac{1}{2}\left[u^{n}_{i,j} + \overline{U^{n+1/2}_{i,j}} - \frac{\Delta t}{vol_{i,j}}\left(\vec{H}^{\overline{n+1/2}}_{i,j+1}\cdot\vec{S}_3 + \vec{H}^{\overline{n+1/2}}_{i,j}\cdot\vec{S}_1\right)\right]$$

Lx operator:

$$\text{predictor} \quad \overline{U^{n+1}_{i,j}} = U^{n+1/2}_{i,j} - \frac{\Delta t}{vol_{i,j}}\left(\vec{H}^{n+1/2}_{i,j}\cdot\vec{S}_4 + \vec{H}^{n+1/2}_{i-1,j}\cdot\vec{S}_2\right)$$

$$\text{corrector} \quad U^{n+1}_{i,j} = \frac{1}{2}\left[U^{n+1/2}_{i,j} + \overline{U^{n+1}_{i,j}} - \frac{\Delta t}{vol_{i,j}}\left(\vec{H}^{\overline{n+1}}_{i+1,j}\cdot\vec{S}_4 + \vec{H}^{\overline{n+1}}_{i,j}\cdot\vec{S}_2\right)\right]$$

$$\vec{S} = \vec{n}S$$

$$\int_S ds = \int_{S_1} ds + \int_{S_2} ds + \int_{S_3} ds + \int_{S_4} ds$$

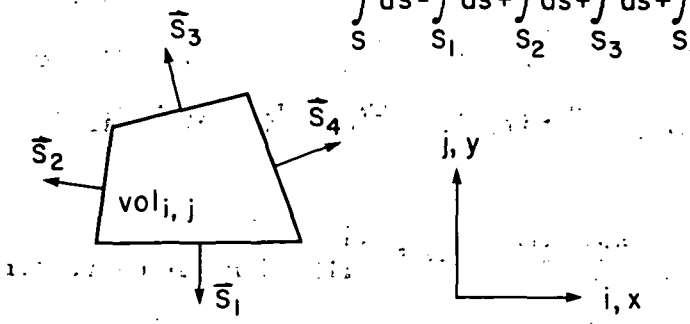

Sketch (a) — Quadrilateral volume element.

The Ly and Lx operators are applied so that equation (1) is satisfied at each time step for each cell of the nonorthogonal nonuniform computational mesh. To evaluate the viscous derivatives for the nonorthogonal mesh, the following transformation is appropriate (ref. 3):

$$\frac{\partial \phi}{\partial x} = \frac{\partial \phi}{\partial \xi}\frac{\partial \xi}{\partial x} + \frac{\partial \phi}{\partial \eta}\frac{\partial \eta}{\partial x} \qquad \frac{\partial \phi}{\partial y} = \frac{\partial \phi}{\partial \xi}\frac{\partial \xi}{\partial y} + \frac{\partial \phi}{\partial \eta}\frac{\partial \eta}{\partial y}$$

where ϕ is a dummy dependent variable, and (ξ,η) are the local coordinates of the nonorthogonal mesh. In terms of the notation in sketch (b),

$$\frac{\partial \phi}{\partial x} = \frac{\Delta\phi_\xi \Delta y_\eta - \Delta\phi_\eta \Delta y_\xi}{\Delta x_\xi \Delta y_\eta - \Delta x_\eta \Delta y_\xi} \qquad \frac{\partial \phi}{\partial y} = \frac{\Delta\phi_\xi \Delta x_\eta - \Delta\phi_\eta \Delta x_\xi}{\Delta y_\xi \Delta x_\eta - \Delta y_\eta \Delta x_\xi}$$

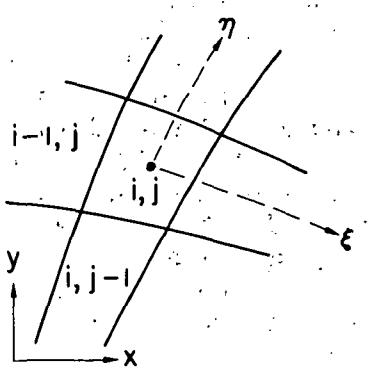

Sketch (b) — Nonorthogonal mesh notation.

For evaluation on surfaces S_3 and S_4, the differences are defined as

$$\Delta\phi_\xi = \phi_{i+1,jj} - \phi_{im,jj} \qquad \Delta\phi_\eta = \phi_{ii,j+1} - \phi_{ii,jm}$$

$$\Delta x_\xi = x_{i+1,jj} - x_{im,jj} \qquad \Delta x_\eta = x_{ii,j+1} - x_{ii,jm}$$

$$\Delta y_\xi = y_{i+1,jj} - y_{im,jj} \qquad \Delta y_\eta = y_{ii,j+1} - y_{ii,jm}$$

and

$$im = \begin{cases} i & \text{for Lx} \\ i-1 & \text{for Ly} \end{cases} \qquad ii = \begin{cases} i & \\ i+1 & \text{for Lx corrector} \end{cases}$$

$$jm = \begin{cases} j-1 & \text{for Lx} \\ j & \text{for Ly} \end{cases} \qquad jj = \begin{cases} j & \\ j+1 & \text{for Ly corrector} \end{cases}$$

This treatment of the viscous derivatives always results in centered differences, maintains second-order accuracy, and provides consistent treatment of discontinuous boundary conditions (such as at the leading and trailing edges of the airfoil).

Control Volume, Mesh, and Boundary Conditions

The airfoil, initially at rest, is impulsively started at time zero at the desired free-stream Mach number and pressure. Figure 1 shows a typical control volume for which the flow-field development is followed in time. At a sufficient distance upstream of the leading edge (in this case six chord lengths), the flow is assumed uniform at the free-stream conditions ($U = U_\infty$) as it is along the far transverse boundary (again, six chord lengths away). The downstream boundary is positioned far enough downstream of the trailing edge (nine chord lengths) so that all gradients in the flow direction may be assumed negligible ($\partial u/\partial x = 0$). The surface of the airfoil is impermeable, and "no slip" boundary conditions are assumed ($u = v = 0$). The airfoil is assumed adiabatic ($\nabla T \cdot \hat{n} = 0$), and the normal surface pressure gradient is zero ($\partial p/\partial n = 0$). Ahead of and behind the airfoil, the flow is symmetric. If the airfoil is thick, and the flow field is transonic, significant boundary-layer separation is likely. To simulate this phenomenon reliably for turbulent flow it is necessary to resolve the boundary layer to the sublayer scale. This sublayer scale is nearly proportional to $1/\sqrt{Re_c}$ so that, for the high Reynolds number flows of interest, the mesh resolution near the surface must be extremely fine. As a rule of thumb, a first mesh spacing of $\Delta y_{min} = 2/3(c/\sqrt{Re_c})$ is adequate.

The mesh used in the studies to date is a 50×38 mesh. In the x-direction, the mesh is uniformly distributed over the surface of the airfoil (20 points) and is exponentially stretched ahead of (10 points) and behind the airfoil (20 points). In the y-direction, a coarse mesh of 26 points is exponentially stretched away from the airfoil. The innermost region is further subdivided

into a medium mesh of 10 exponentially stretched points and a fine mesh of 4 uniformly spaced points.

Turbulence Model

The turbulence modeling is incorporated in the shear stress term τ_{xy} and τ_{yx} in the form of an eddy-viscosity coefficient ε as

$$\tau = \tau_{xy} = \tau_{yx} = (\mu + \varepsilon)\left(\frac{\partial u}{\partial y} + \frac{\partial v}{\partial x}\right)$$

Two different algebraic models have been considered, each expected to perform adequately ahead of the shock-wave—boundary-layer interaction regions but to exhibit different behavior when the flow separates.

The first model considered (model 1) is a van Driest formulation (ref. 4) for the wall region and a plane mixing formulation for the outer region. No special consideration is given to separated regions and the airfoil wake is described by a Clauser (ref. 5) wake formulation.

Wall Region:

$$\varepsilon = \rho \ell^2 \left|\frac{\partial u}{\partial y} + \frac{\partial v}{\partial x}\right|$$

$$\ell = 0.4y\left[1 - \exp(-y/A)\right]$$

$$A \equiv 26 \frac{\mu_w}{\rho_w}\sqrt{\frac{\rho_w}{|\tau_w|}}$$

Outer Region:

$$\varepsilon = \rho \ell^2 \left|\frac{\partial u}{\partial y} + \frac{\partial v}{\partial x}\right|$$

$$\ell = 0.07(\delta - y_o)$$

where δ is the boundary-layer thickness and y_o is the furthest point across the boundary layer where the velocity is zero. (For attached boundary layers $y_o = 0$.)

Airfoil Wake:

$$\varepsilon = 0.001176\rho(\delta - y_o)\left|u_\delta - u_{\mathfrak{L}}\right|$$

where u_δ is the velocity at the edge of the wake and $u_{\mathfrak{L}}$ is the velocity at the center line.

Prandtl Number:

$$Pr = Pr_t = 0.90$$

The second model (model 2) uses a van Driest formulation for the wall region and a Clauser formulation with an intermittency factor in the outer region. A limiting minimum value is imposed on velocity gradient used in the separation-bubble description and the airfoil wake is described by the boundary-layer-wake formulation.

Wall Region:

$$\epsilon = \rho \ell^2 \left[\left(\frac{\partial u}{\partial y} \right)^2 + \left(\frac{\partial v}{\partial x} \right)^2 \right]^{1/2}$$

$$\ell = 0.41y \left[1 - \exp(-y/A) \right]$$

$$A \equiv 26 \frac{\mu_w}{\rho_w} \sqrt{\frac{\rho_w}{|\tau_w|}}$$

Outer Region:

$$\epsilon = \frac{0.0168 U_\delta \delta_i^*}{1 + \left[(y - y_o)/\delta \right]^6}$$

$$\delta_i^* = \int_{y_o}^{\delta} \left(1 - \frac{u}{u_\delta} \right) dy$$

Separation Bubble: Same as wall region except that

$$\left[\left(\frac{\partial u}{\partial y} \right)^2 + \left(\frac{\partial v}{\partial x} \right)^2 \right]^{1/2} \geq \frac{u_\delta}{\delta}$$

Airfoil Wake: Same as outer region

Prandtl Number:

$$Pr = 0.72 , \qquad Pr_t = 0.90$$

The validity of each of these models in the interaction and separated flow regions is highly suspect and requires verification by experiment. While it may be necessary to resort to more rigorous turbulent models in these regions, the simple models used here should permit some insight into the influence of viscosity on such flow fields and are adequate for the early development stages of the computer codes.

Computational Time Step

Six different computational time steps are used in the calculation; one for the Lx operator and one for the Ly operator in each of the three mesh regions. Each time step is determined by the CFL (Courant-Friedrichs-Lewy) and viscous stability requirements from the following relation:

$$\Delta t = \frac{h}{|V| + a + (\alpha/h)(\mu + \varepsilon)/\rho}$$

where h is the appropriate mesh spacing, V is the appropriate velocity component, a is the local speed of sound, and α is a function of the mesh aspect ratio. In the fine mesh in the wake behind the airfoil, the eddy viscosity ε is quite large, and the viscous stability criterion may govern the time step for the Ly operator. To avoid this undesirable restriction and unneeded resolution of the wake, the entire fine mesh region downstream of the airfoil is averaged and treated as part of the medium mesh.

VALIDATION

Because computations of this complexity have not previously been performed, the validity of the present code has been determined by comparison with established computations for certain specific regions of the flow field and with experimental results obtained in the Ames High Reynolds Number Channel.

Inviscid Flow Field

The viscous terms were neglected and the inviscid flow was computed over a 6-percent circular-arc airfoil at a free-stream Mach number of 0.90. The surface pressure distribution is compared in figure 2 with a computation using the small-disturbance-theory program of E. M. Murman of Flow Research, Inc. (refs. 6 to 8 and unpublished information) and an Euler equation computation by R. W. MacCormack of Ames Research Center. Both of these computations employed special considerations at the shock which have not been incorporated in the present code. The agreement between the three computations (all of which solve the conservative form of the equations) is excellent.

Attached Boundary Layer

The flow over an 18-percent-thick circular-arc airfoil at a free-stream Mach number of 0.775 and a chord Reynolds number of 2×10^6 was computed using eddy-viscosity model 1. The computed surface pressure distribution was input to the turbulent boundary-layer code of Marvin and Sheaffer of Ames Research Center (ref. 9 and additional information supplied by Marvin) which uses an implicit Crank-Nicholson method and a Cebeci-Smith eddy-viscosity model (ref. 10). Computed values of local skin friction from this boundary-layer code are compared with the present calculation in figure 3. Ahead of the

separated-flow region the agreement is excellent except for a small region near the leading edge where the Marvin-Sheaffer code assumes a laminar to turbulent transition region.

In addition to skin friction, boundary-layer velocity profiles computed by the present code are compared in figure 4 with the compressible form of the universal "law of the wall." Here the symbols represent the numerical solution and are plotted at y^+ values corresponding to the mesh centers. All profiles are seen to have one point in the sublayer and adequately describe the log-law and wake-flow regions of the boundary layer.

Experimental Comparisons

Surface-pressure measurements, oil-flow studies, and shadowgraph studies were made using an 18-percent-thick circular-arc airfoil in the Ames High Reynolds Number Channel. Chord Reynolds numbers were varied between 1 and 13 million for free-stream Mach numbers between 0.711 and 0.788. In these experiments, flow-field streamlines, determined from the present computer code, were used to design contoured tunnel walls in an attempt to minimize tunnel interference effects.

Figure 5 shows a comparison between experimental and computed surface pressure distributions over the 18-percent-thick circular-arc airfoil at $M_\infty = 0.775$ and $Re_c = 2\times10^6$. Three computed distributions are shown in this figure as determined by the present code. One of these is an inviscid calculation, and the other two were determined using eddy-viscosity models 1 and 2. All comparisons are in excellent agreement ahead of the interaction region. Both viscous computations show a marked improvement over the inviscid results in the interaction region. The solution with model 2 shows the best agreement with experiment with respect to shock location and shock strength. Both viscous solutions indicate a shock-induced separation with the separation bubble extending into the wake. This is denoted in figure 5 by the pressure plateau downstream of the 80-percent-chord point. The experimental pressure distribution does not indicate this extensive separation region, and herein constitutes the greatest disagreement between computation and experiment. As will be shown later, at this particular choice of free-stream Mach number the experimental flow field can be highly unsteady, and direct comparisons in the separated flow region may be invalid.

The first study performed using the code was to assess the influence of Reynolds number on the transonic flow field. Using the 18-percent circular arc at $M_\infty = 0.775$, the chord Reynolds number was parametrically varied from 1×10^6 to 6.67×10^6 and the flow field computed using eddy-viscosity model 1. The results of this study are shown in figure 6 for the surface pressure distribution. Included for reference is the inviscid solution. Three features are apparent in this figure. First the influence of Reynolds number on this flow field is small while the effect of viscosity is large. Second, as the Reynolds number is decreased, the shock strength decreases and the shock moves forward on the airfoil. And third, as the Reynolds number is decreased, the displacement effects in the separation region increase resulting in less pressure recovery near the trailing edge. The displacement effect ahead of the

interaction region is nearly the same for the entire Reynolds number range considered.

A similar study was performed experimentally. Figure 7 shows the measured surface pressure distributions over an 18-percent circular-arc airfoil at $M_\infty = 0.750$. Except for boundary-layer-transition effects at the lower Reynolds number, the experimental study bears out the same conclusions determined from the numerical results. In addition to Reynolds number effect, the influence of free-stream Mach number was also experimentally studied. Figure 8 shows measured surface pressure distribution over an 18-percent circular-arc airfoil at $Re_c = 10 \times 10^6$. Results for four free-stream Mach numbers are included: $M_\infty = 0.74$, 0.76, 0.77, and 0.79. At $M_\infty = 0.74$ the flow is nearly subcritical and the shock is very weak. For $M_\infty = 0.76$ the shock is much stronger but there is still a large pressure recovery at the trailing edge, indicating small separation effects. For $M_\infty = 0.77$ there is a dramatic shift in pressure distribution over the aft portion of the airfoil. This sudden jump is associated with the shock-induced separation merging with existent trailing-edge separation, resulting in a large reverse flow region and large boundary-layer displacement effects. This phenomenon persists at the higher free-stream Mach numbers. This Mach number dependence of onset of massive separation is also a function of Reynolds number, which is discussed in reference 11.

To understand this discontinuous dependence on Mach number, shadowgraph movies were made of the flow over the aft portion of the airfoil as the Mach number was varied through the critical range. Photographs of selected frames of one such film are shown in figure 9 for an 18-percent circular-arc airfoil at $Re_c = 7 \times 10^6$. The Mach number variation is from 0.76 to 0.79 and results are shown for values of 0.76, 0.77, and 0.79. At $M_\infty = 0.76$ the flow is steady and there is some separation at the trailing edge. As the Mach number is increased, the flow becomes unsteady, switching alternately from massive separation to fully attached or small trailing-edge separation. This unsteadiness is most probably an asymmetric phenomenon; hence it is not reasonable to expect to simulate this phenomenon with a symmetric, free boundary code. When the Mach number reaches 0.79, the flow is again steady with massive shock-induced separation. Note that at the lower Mach number the shock is fairly weak and nearly normal to the airfoil surface. At the higher Mach number the shock is stronger and is definitely oblique — probably a lambda shock.

To avoid comparisons in the unsteady flow regimes, subsequent computations were performed only for the lower and higher Mach numbers where the experimental flow is known to be steady. In addition, because of the superior performance indicated in figure 5 of eddy-viscosity model 2 versus eddy-viscosity model 1 in the interaction regime, model 1 has been dropped from further consideration.

Oil-flow photographs of both the low and high Mach number experimental steady-flow regimes are shown in figure 10. At $M_\infty = 0.76$ the line at the

onset of trailing-edge separation is clearly indicated by the oil flow. The symmetry of the separation bubble is indicated in the right-hand photograph of the junction of the airfoil trailing edge and the tunnel side wall. At $M_\infty = 0.79$ the onset of shock-induced separation is indicated. The right-hand photograph of the junction of the airfoil trailing edge and the tunnel side wall clearly indicates the magnitude of the separation bubble. The photographs in figure 10 also serve to indicate the two-dimensional and symmetric character of the flow.

For a chord Reynolds number of 4×10^6 the flow field over the 18-percent circular-arc airfoil was simulated using eddy-viscosity model 2 for $M_\infty = 0.742$ and $M_\infty = 0.788$, corresponding to the two extremes of the experimental steady flows. Figure 11 shows a comparison with experimental data of the surface pressure distributions for the two cases. In figure 11(a) the viscous solution is an improvement over the inviscid result but does not agree with the experiment in the shock—boundary-layer interaction region. The experiment indicates a stronger influence of viscosity than does the calculation, resulting in a weaker, more smeared out shock. Near the trailing edge, however, the agreement is better, both distributions supporting the fact that there is only trailing-edge separation and both indicating the same level of pressure recovery. The reason for the substantial disparity in the interaction region is not yet clear. It may be related to the fact that the shock is near the midchord and, for a chord Reynolds number of only 4×10^6, the boundary layer may actually be transitional in that region. This could lead to the stronger viscous-inviscid interaction effect indicated by the experiment.

In figure 11(b) the viscous solution again is an improvement over the inviscid result. Here the agreement between experiment and viscous calculation is good in the interaction region but is poor over the separation bubble. Unfortunately, there was no experimental data for $Re_c = 4\times10^6$ at $M_\infty = 0.788$ so data are shown for $Re_c = 2\times10^6$ and 7×10^6. It is expected that data for 4×10^6 will fall within the envelope defined by these two limits. Note that both the experimental and calculated pressures tend to plateau over the separation bubble and indicate a similar extent over the aft portion of the airfoil. The computed pressures indicate larger recovery in this region and, as will be seen in the next figure, this is associated with the fact that the shock wave in the experiment is oblique while that simulated is nearly normal. The fundamental reason for this disparity is not yet clear but it is likely attributable to the inability of the simple eddy-viscosity model to support this complicated flow.

Figure 12 shows the flow field detail over the aft portion of the airfoil for the two Mach numbers considered above. The top photographs are shadowgraphs of the experiment. For $M_\infty = 0.742$ the shock is weak and normal to the surface. Separation occurs only at the trailing edge and is small in extent. For $M_\infty = 0.788$ the shock is strong and oblique. Separation is shock induced and extends into the wake. Immediately beneath the photographs are computed Mach number contours. For $M_\infty = 0.742$ the flow features are quite similar to the shadowgraph above. For $M_\infty = 0.788$ the shock is seen

to be nearly normal to the surface as opposed to being oblique in the shadowgraph, but the magnitude of the separated flow region is similar to that shown in the shadowgraph. The bottom part of this figure contains computed velocity vector plots showing the details of the separation bubbles and the effect of the shock in retarding the flow. Subsequent experiments using a laser velocimeter are planned to provide similar experimental data in this region.

COMPUTER REQUIREMENTS

The present code was originally written in FORTRAN and debugged on an IBM 360/67 using the interactive features of the time sharing system. Subsequently, it was run on the CDC 7600, requiring 2 to 10 hours per converged solution, depending on chord Reynolds number. Because of the long run times, the code was completely restructured and written in the vector-oriented Ames-developed CFD language.[1] This code was translated to assembly language for the ILLIAC IV and to FORTRAN for the CDC 7600. The resulting FORTRAN code was further optimized, using COMPASS coded subroutines for *all* vector arithmetic operations. Resultant run times are now 0.8 to 4.2 hours per converged solution on the CDC 7600, and 0.6 to 3.0 hours on the ILLIAC IV. There is substantial room for speed increase on the ILLIAC IV in that (1) the quoted run times were for the ILLIAC operating at 11.5 MHz instead of the design speed of 15-16 MHz, (2) the ILLIAC was operated in non-overlap mode, and (3) each iteration was performed twice and the solutions compared before continuing with the computation. Each of these areas represents potential speed reductions of 0.72, 0.40, and 0.48, respectively, leading to an overall potential speed reduction of 0.14. In this case, the present code would require from 0.08 to 0.42 hour per converged solution — an order of magnitude faster than the vector-coded CDC 7600.

CONCLUDING REMARKS

In conclusion, a code has been written to simulate transonic turbulent flow fields over two-dimensional bodies of arbitrary configuration. At present, only algebraic eddy-viscosity models have been considered to achieve turbulence closure. With these models the code yields valid solutions in the inviscid flow field and in the attached boundary layer ahead of interaction regions. The validity of the numerical simulations in the shock—boundary-layer interaction region and in reverse flow regions is directly related to the turbulence model. For the models considered thus far, comparisons with experiment have been less than good. This is to be expected since the models are developed from flat-plate incompressible boundary-layer data. Nevertheless, the viscous solutions represent a considerable improvement over inviscid solutions and do predict the proper features of the flow.

---

[1] Computational Fluid Dynamics (A FORTRAN-Based Language for the ILLIAC IV developed at Ames Research Center in 1973).

The code has been optimized for the CDC 7600 computer and requires from 0.8 to 4.2 hours to simulate the transonic flow field over an 18-percent circular-arc airfoil. The code has also been written for the ILLIAC IV and presently requires from 0.6 to 3.0 hours to simulate these transonic flows. These ILLIAC run times have a potential reduction to 0.08 to 0.42 hour, if total advantage is taken of certain design features of the ILLIAC.

REFERENCES

1. MacCormack, R. W.: Numerical Solution of the Interaction of a Shock Wave with a Laminar Boundary Layer. Lecture Notes in Physics, vol. 8, Springer-Verlag, pp. 151-163.

2. MacCormack, R. W., and Paullay, A. J.: Computational Efficiency Achieved by Time Splitting of Finite Difference Operators. AIAA Paper 72-154, 1972.

3. Deiwert, G. S.: Numerical Simulation of High Reynolds Number Transonic Flows. AIAA Paper 74-603, June 17-19, 1974.

4. Van Driest, E. R.: On Turbulent Flow Near a Wall. Jour. Aero. Sci., vol. 23, 1956, p. 1007.

5. Clauser, F. H.: The Turbulent Boundary Layer. Adv. in App. Mech. IV, pt. 1, New York, Academic Press, 1956.

6. Murman, E. M., and Cole, J. D.: Calculation of Plane Steady Transonic Flows. AIAA Jour., vol. 9, no. 1, 1971, pp. 114-121.

7. Murman, E. M.: Analysis of Embedded Shock Waves Calculated by Relaxation Methods. Proc. AIAA Computational Fluid Dynamics Conference, 1973, pp. 27-40.

8. Murman, E. M.: Computation of Wall Effects in Ventilated Transonic Wind Tunnels. AIAA Paper 72-1007, 1972, pp. 216-217.

9. Marvin, J. G., and Sheaffer, Y. S.: A Method for Solving the Nonsimilar Laminar Boundary-Layer Equations Including Foreign Gas Injection. NASA TN D-5516, 1969.

10. Inouye, M., Marvin, J. G., and Shaeffer, Y. S.: Turbulent-Wake Calculations with an Eddy-Viscosity Model. AIAA Journal, vol. 10, no. 2, 1972.

11. McDevitt, J. B., Levy, L. L., and Deiwert, G. S.: Transonic Flow About Thick Circular-Arc Airfoils. AIAA Paper 75-875, 1975.

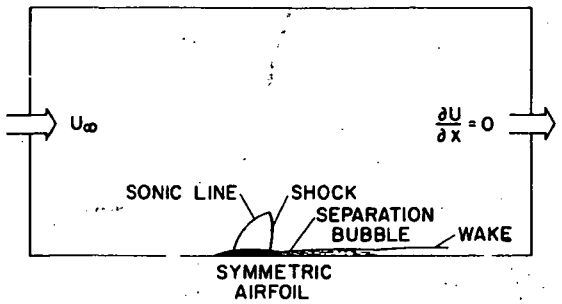

Figure 1.— Computational control volume.

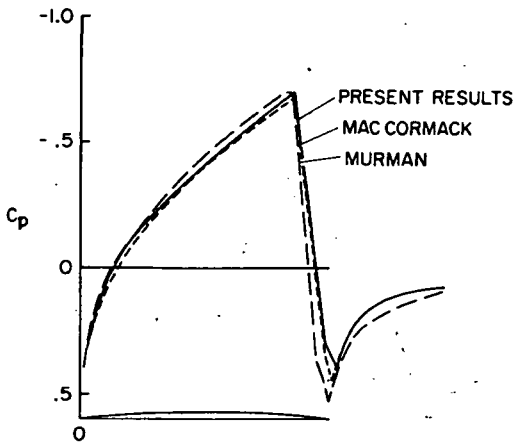

Figure 2.— Inviscid pressure distribution over a 6-percent circular-arc airfoil; $M_\infty = 0.90$.

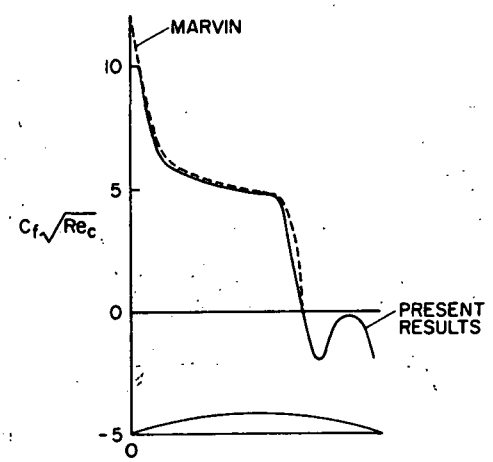

Figure 3.— Skin-friction distribution over an 18-percent circular-arc airfoil; $M_\infty = 0.775$, $Re_c = 2\times10^6$.

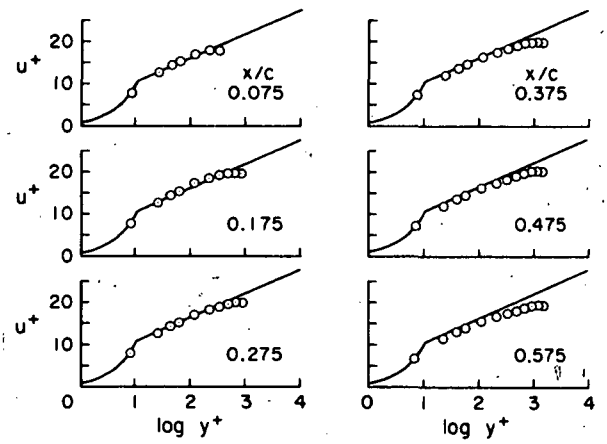

Figure 4.— Velocity profiles ahead of shock; $M_\infty = 0.775$, $Re_c = 2\times10^6$.

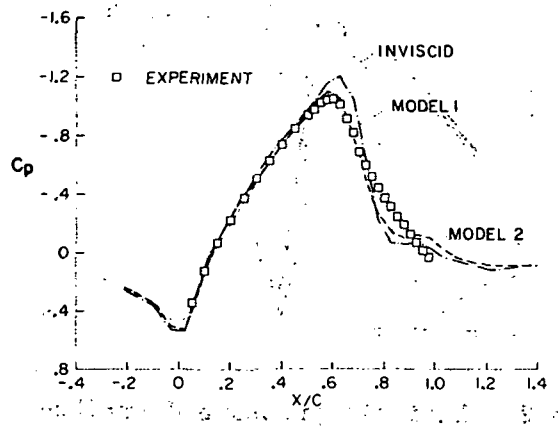

Figure 5.— Pressure distribution over an 18-percent circular-arc airfoil; $M_\infty = 0.775$, $Re_c = 2\times10^6$.

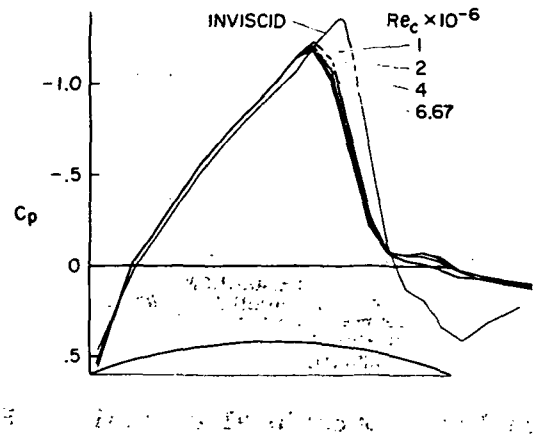

Figure 6.— Pressure distribution over an 18-percent circular-arc airfoil; $M_\infty = 0.775$.

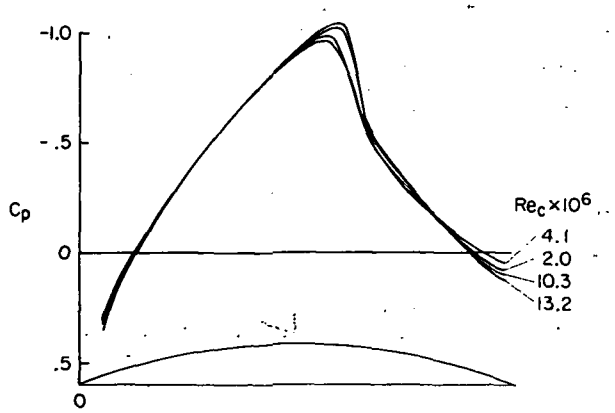

Figure 7.— Experimental pressure distribution over an 18-percent circular-arc airfoil; Reynolds number effect, $M_\infty = 0.750$.

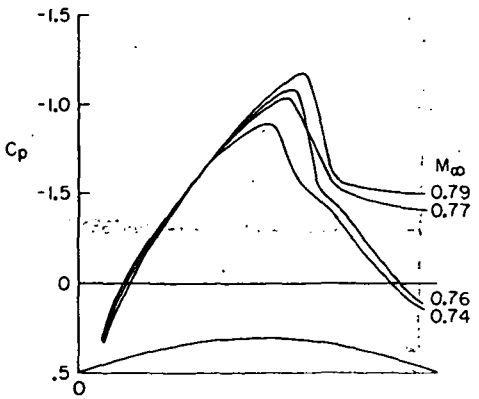

Figure 8.— Experimental pressure distribution over an 18-percent circular-arc airfoil; Mach number effect, $Re_c = 10\times10^6$.

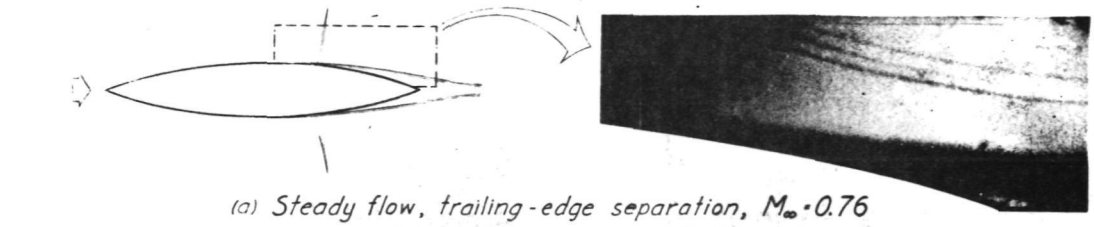

(a) Steady flow, trailing-edge separation, $M_\infty = 0.76$

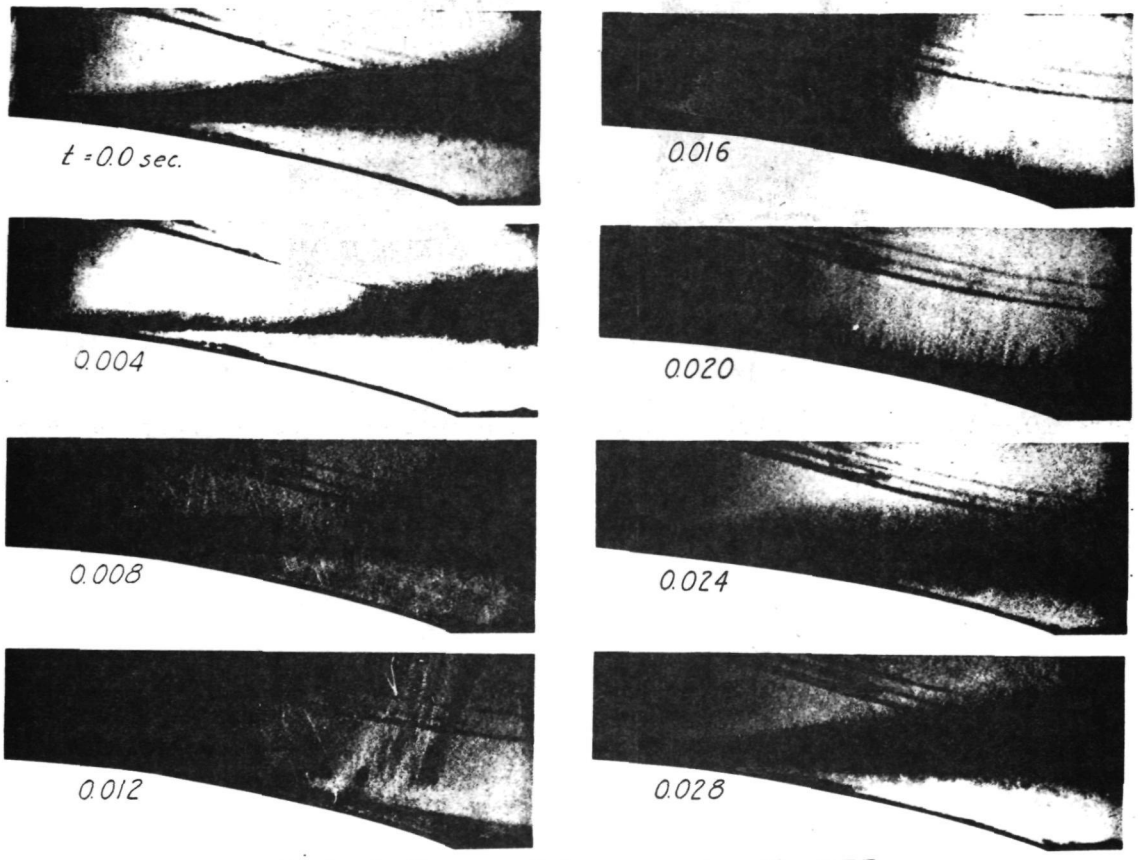

(b) Unsteady flow, oscillatory separation, $M_\infty = 0.77$

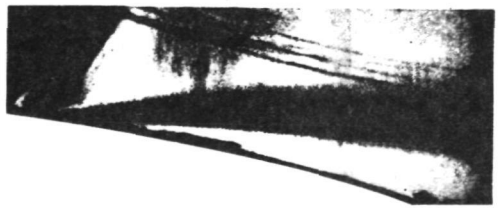

(c) Steady flow, shock-induced separation, $M_\infty = 0.79$

Figure 9.— Photographs of boundary-layer separation from a shadowgraph movie; $t/c = 0.18$, $Re_c = 7 \times 10^6$.

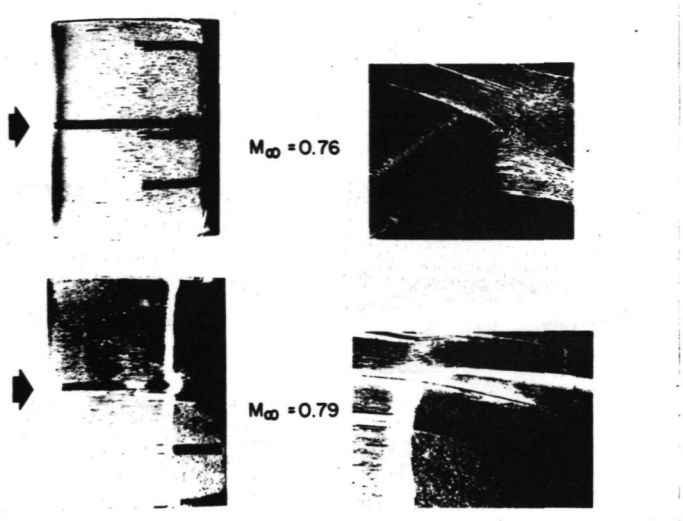

Figure 10.— Oil-flow patterns of separation regions; t/c = 0.18, $Re_c = 10\times10^6$.

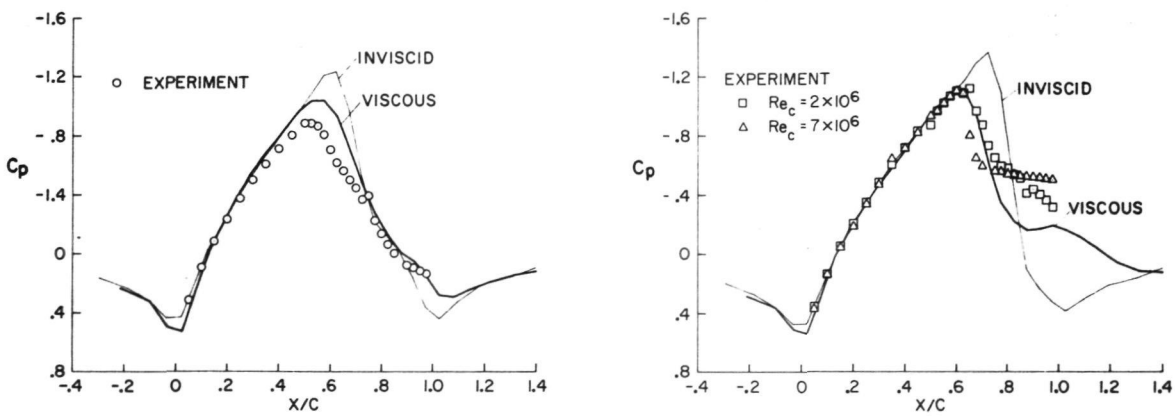

(a) $M_\infty = 0.742$.

(b) $M_\infty = 0.788$.

Figure 11.— Pressure distributions over an 18-percent circular-arc airfoil; $Re_c = 4\times10^6$.

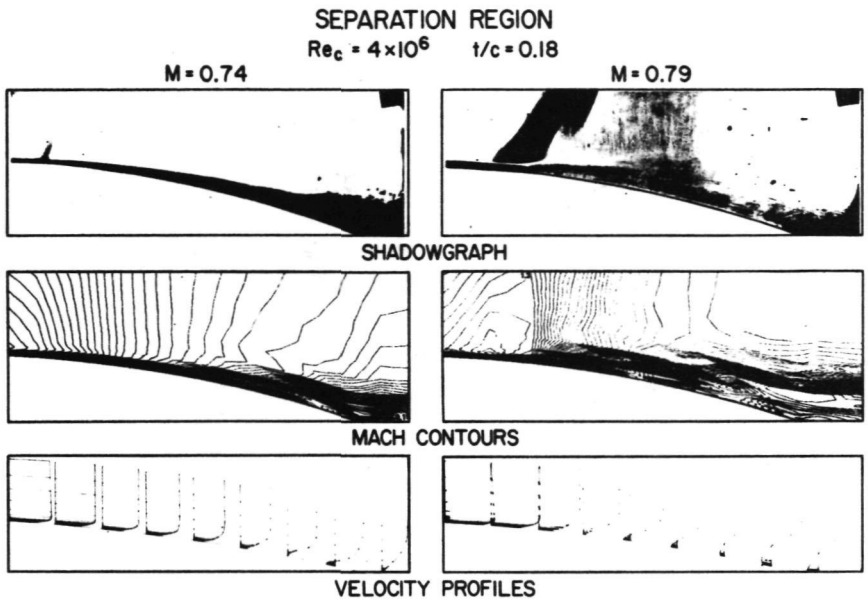

Figure 12.- Flow-field details over the aft portion of an 18-percent circular-arc airfoil.